Particles control in selective laser melting in-situ oxide dispersion strengthened method

Xin Zhou[1], Zhibin An[1,4], Zhijian Shen[2], Wei Liu[2], Chenguang Yao[3]

[1]Science and Technology on Plasma Dynamics Laboratory, 710038, Xi'an, China
[2]School of Materials Science and Engineering, Tsinghua University, 100084, Beijing, China
[3]China Women's University, 100101, Beijing, China

E-mial: azb1999@163.com

Abstract. Stainless steel selective laser melting (SLM) can be considered as a new possible approach for in-situ formation of oxide dispersion strengthened (ODS) steels because of the dispersion of amorphous oxide nano-particles due to the trace amounts of laser chamber oxygen and in-situ internal oxidation of reactive elements. In this paper it is demonstrated that the particle sizes and distributions can be adjusted by choosing different chamber oxygen level through controlling the quantity of initial reactive cores and the available reactive solutes of each core.

1. Introduction

The in-situ formation of oxide nano-particles during 316L stainless steel selective laser melting (SLM) has been reported in [1-3]. It is considered as a possible approach for in-situ formation of ODS-steels (Oxide Dispersion Strengthened) where the constituents of Si and Cr readily react with oxygen presented inside the 316L steel powder and the laser chamber. Saeidi reported that the ODS SLM 316L steel achieved a higher tensile strength (703 MPa) and a higher yield strength (456 MPa) compared to that of the conventionally casted 316L steel (620MPa and 310 MPa, accordingly), and a higher ductility with 46% elongation compared to that of HIPed ODS 304 steel (20~25%) and cast 316L (30%) [1].

A uniform and controlled dispersion of second phase particles is very critical in the material performance, ODS alloys commonly employ a high energy ball milling technique but it is time-consuming [4]. The internal oxidation process is another possible ODS method involving selective reactions of a less noble solute with oxygen [5, 6]. The in-situ formation of ODS-steels through SLM belongs to the category of internal oxidation and includes two basic physical steps: one is the formation and growth of oxide particles and the second is the dispersion of formed particles under laser driven strong convections. The fluid flow characteristics and particle migration behaviors within the melt pool are well reported in SLM and/or laser welding [7-11], then uniform dispersions of second phase particles can be expected under proper laser parameters.

The growth kinetics and size control of oxide nano-particles are another research hot spots. The particles growth is controlled by the mechanism of "reactive crystallization", "diffusion-controlled precipitation" and "collisional growth" in melt pool [12]. The growth rate is proportional to the initial oxygen concentration, the melt flow field intensity and the particle collision probability, therefore the sizes and distributions of nano-particles can be adjusted by manipulating the chamber oxygen level. In

this paper, 316L selective laser melting experiments are conducted with different chamber atmosphere (different oxygen levels) then the sizes, distributions and constituents of oxide nano-particles are analyzed, the forming mechanism and growth behavior are also discussed.

2. Material and methods

316L stainless steel powder granules with an overall chemical composition of 17 wt.% Cr, 10.6 wt.% Ni, 2.3 wt.% Mo, 0.98 wt.% Mn, 0.5 wt.% Si, 0.5 wt.% Ti, and Fe being the balance was used as precursor, supplied by Renishaw (Renishaw, Shanghai, China). SLM experiments were conducted at a Renishaw AM250 facility (Renishaw AMPD, Stone, UK) with laser parameters of power 190W, scan speed 700 mm/s, line spacing 0.05 mm, and "zigzag" scan strategy. The chamber residual oxygen contents in Ar atmosphere were set as extreme low (＜50ppm), medium (300~500ppm), and high (1000~1200ppm) respectively. TEM observations were conducted on a JEM-2100 microscope (JEOL, Tokyo, Japan) and the sample preparation followed the procedures in [2].

3. Results and discussion

As predicted, no oxide particles can be found in the microstructure in extreme low oxygen (less than 50ppm) chamber environment and the dislocations are non-uniform, Figure 1 (a ~ b). Increasing the chamber oxygen level to 300~500ppm, some large oxide particles can be formed with size around 500 nm~2 μm, Figure 1 (d) and Figure 2 (a ~ b). The quantity of oxide particles is limited at this oxygen level but plenty of dislocations and the pinning effects of particles can be clearly observed. With further increase of the chamber oxygen level to 1000~1200 ppm, oxide nano-particles of size 50~100 nm are dispersive and distributed homogeneously, Figure 1 (c). The particles in 1000 ppm oxygen level are fairly accorded with results reported in former literatures. Based on EDS analysis, the inclusion constituents are actually Fe, Ni, Cr, Ti and Si oxides, Figure 2 (c), the Cr, Ti, Si and O elements are relatively high but the Ni element is lower compared with the matrix Ni content, Figure 2 (d). This implies the oxide particles have similar chemical constitutions and amorphous structures (presented in [1]) with stainless steel oxide (passive) films which are not the harmful brittle phases, such as σ (tetragonal), $M_{23}C_6$ (FCC) or χ phase (BCC). Thus the following conclusions can be made: the formation of nano-particles is closely related to the oxygen environment and with an increase in the chamber oxygen level, the particle size reduces but the particle distribution is more dispersed. The particle size discrepancy can be as high as 40 times in different chamber oxygen content, 50 nm in 1000 ppm while 2 μm in 300~500 ppm, Figure 1(c, d).

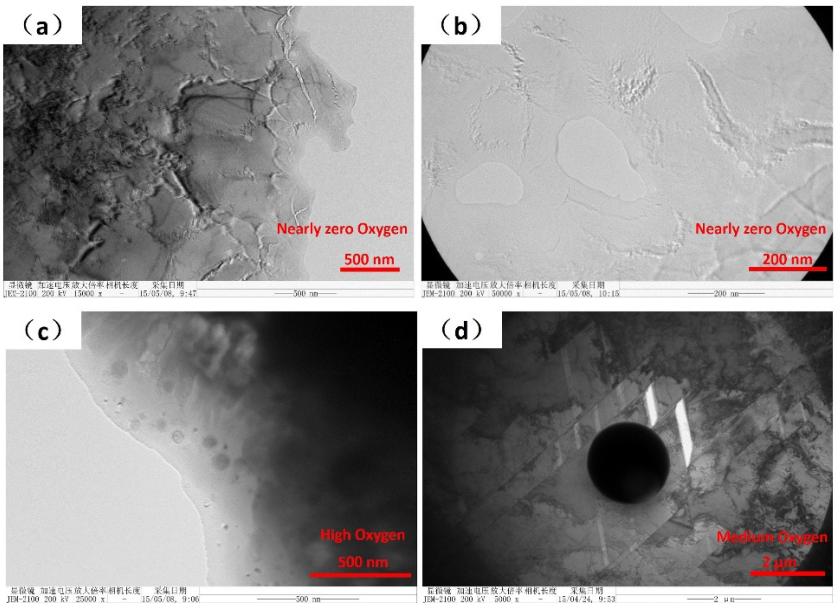

Figure 1. The distribution of oxide particles, chamber oxygen level of less than 50ppm (a ~ b), 1000~1200ppm (c), and 300~500ppm (d).

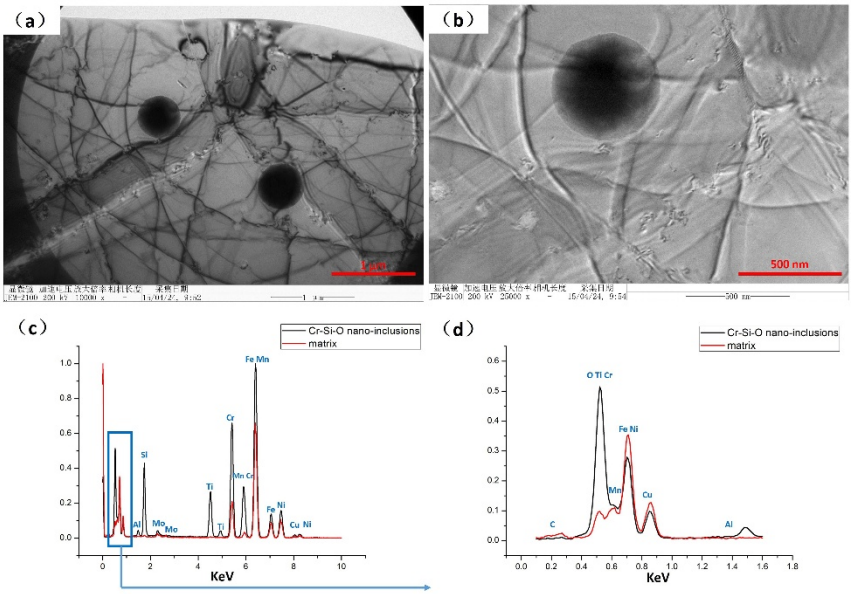

Figure 2. The oxide particles formed in the chamber oxygen level of 300~500ppm (a, b). EDS spectrums of a nano-inclusion and the matrix (c), the partial enlarged view of 0~1 KeV (d).

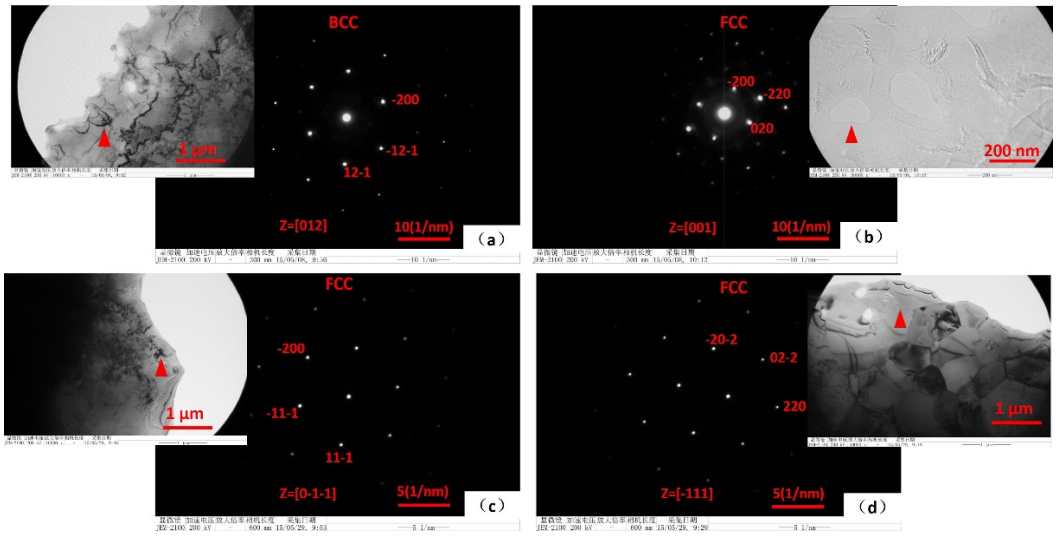

Figure 3. TEM analysis and corresponding electron diffraction patterns.

(a) and (b) with extreme low oxygen less than 50ppm, (c) and (d) with high oxygen 1000~1200 ppm. The diffraction positions taken in (a) and (c) are with high density dislocations, while in (b) and (d) are with nearly no dislocations.

The chamber oxygen level can affect not only the inclusion formations but also the matrix microstructures. As shown in Figure 3 the TEM analysis and corresponding electron diffraction patterns in extreme low oxygen chamber environment, most areas can be identified as the FCC structures (austenite) but some areas with high density dislocation tangles can be identified as the BCC structures demonstrating the ferrite nucleation. In a high oxygen environment (1000~1200 ppm), all

the diffraction regions regardless of dislocation densities are all identified as the FCC structures (austenite).

316L stainless steel solidifies as the main austenite but a small amount of ferrite can be generated through eutectic reaction in the cellular/dendritic interface according to its constituents and phase diagram. Austenite stabilizing elements (e.g. Ni) will be consumed during laser melting and the re-solidifying process, while ferrite stabilizing elements (e.g. Si, Cr, Ti, and Mo) will be enriched in the solidification front and dendritic interface. With low oxygen chamber atmosphere, in this local area of dendritic interface the equivalent proportion of Cr and Ni (Cr_{eq}/Ni_{eq}) will be increased which will then form ferrite nucleation and high density dislocations, Figure 3 (a). With a certain amount of oxygen in the chamber, a thin oxide film on the melt pool surface will be generated rapidly by oxidation of the rejected Ti, Si and Cr for the high laser irradiation temperature and shallow melt pool (100~200 μm depth). Moreover, melt convection in the laser melt pool is another significant feature [8, 13] and under this strong stirring action the formed oxide film will be scattered and then dispersively distributed in the microstructure as the discovered oxide nano-particles. For Ni the element is consumed by austenitic solidification, so it's counting is a bit lower in oxide-particles than in the matrix. Cr, Ti and Si are excessively consumed by oxidation, so ferrite nucleation seems impossible in high oxygen chamber atmosphere. Mo element (solute) is heavier than Fe melt (solvent) and does not participate in the formation of oxide film [14], so it will be distributed in the cellular boundaries.

There still remains difficulty in calculating the particle sizes and distributions quantitatively because of the lack of some thermophysical data, but the qualitative analysis based on growth kinetics of particles can be still involved. Nano-particles in laser melt pool can be considered as a polydisperse system with a radius of a continuous distribution, the density distribution function of particles $n(r)$ is defined as a steady-state exponential distribution in particle radius range (r, $r+dr$) [15]:

$$n(r)=n_0 \exp(-\lambda r),\ r_0 < r < r_1 \tag{1}$$

The parameters n_0, λ, r_0, r_1 are decided by specific experimental conditions, where

$$n_0 = \frac{3\rho_f[\mathrm{o}\%]}{4\pi\rho_p X_o \int_{r_0}^{r_1} r^3 e^{-\lambda r} dr} \tag{2}$$

[O%] is the oxygen content in the melt, X_o is the oxygen mass fraction in particles. Therefore the particle number density is directly correlated with oxygen level, the higher oxygen level in laser chamber and the higher dissolved oxygen in the melt (*[O%]*), means more amounts of oxide particles (n_0 and $n(r)$) can be generated.

Based on sphere diffusion model [12], the maximum radius R_∞ of oxide-particles growth is defined as:

$$R_\infty = R_d \frac{(\mathrm{c}_0 - \mathrm{c}_\mathrm{p})^{1/3}}{c_p^{1/3}} \tag{3}$$

Where R_d is the radius of sphere diffusion (Figure 4 b ~ c), C_o is initial concentration of reactive elements (Cr, Si, Ti, O, etc.) in the melt, C_p is mass fraction of reactive elements in the particles. Therefore, the maximum radius R_∞ is controlled by the number of reactive cores and diffusion radius R_d. Higher density of initial reactive cores ($n(r)$) decides the shorter diffusion radius R_d which means the available solute for each reactive core is limited.

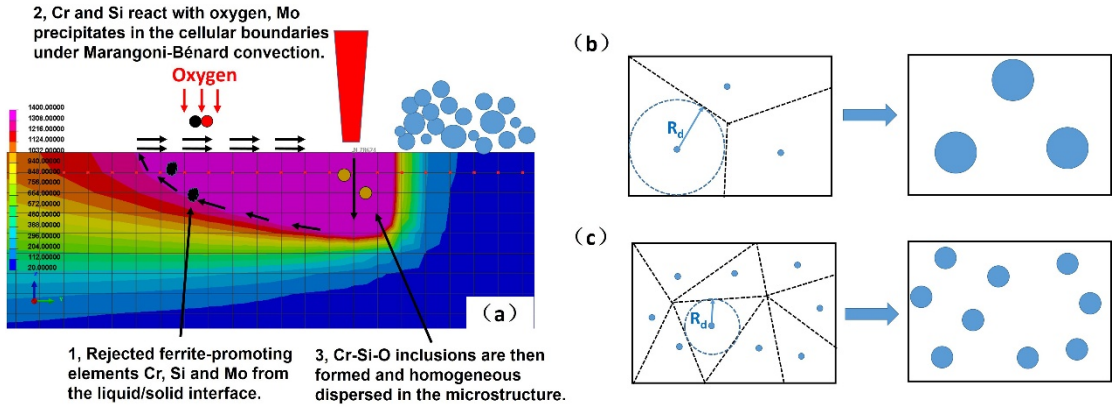

Figure 4. The formation mechanism of oxide particles (a). (b) and (c) exhibit the scenarios of different oxygen level, 300~500ppm and 1000~1200ppm separately.

4. Conclusions

Based on these analyses, oxygen level can be used as a regulating method. Therefore, the quantity of initial reactive cores is limited and oxide-particle growth is sufficient in the condition of 300~500 ppm chamber oxygen. On the contrary, the initial reactive cores are numerous and the final radius is limited in the condition of 1000~1200 ppm chamber oxygen. Higher oxygen content may further reduce the particle size but high oxygen level (over 1500ppm) will deteriorate SLM densities because of the balling phenomenon [16]. Adding small amounts of Ti, Al and Y and fabricating in an atmosphere of 300~500ppm oxygen can be predicted as a new possible process for in-situ ODS 316L steel.

References

[1] K. Saeidi, L. Kvetkova, F. Lofajc, Z. Shen, Austenitic stainless steel strengthened by the in situ formation of oxide nanoinclusions, *RSC ADV* **5**(2015) 20747-20750.
[2] K. Saeidi, X. Gao, Y. Zhong, Z.J. Shen, Hardened austenite steel with columnar sub-grain structure formed by laser melting, *MAT SCI ENG A-STRUCT* **625**(2015) 221-229.
[3] K. Saeidi, X. Gao, F. Lofaj, L. Kvetkova, Z.J. Shen, Transformation of austenite to duplex austenite-ferrite assembly in annealed stainless steel 316L consolidated by laser melting, *J. ALLOY COMPD* **633**(2015) 463-469.
[4] A. Chauhan, D. Litvinov, J. Aktaa, High temperature tensile properties and fracture characteristics of bimodal 12Cr-ODS steel, *J. NUCL MATER* **468**(2016) 1-8.
[5] M. Hansel, C.A. Boddington, D.J. Young, Internal oxidation and carburisation of heat-resistant alloys, *CORROS SCI* **45**(2003) 967-981.
[6] M. Udyavar, D.J. Young, Precipitate morphologies and growth kinetics in the internal carburisation and nitridation of Fe-Ni-Cr alloys, *CORROS SCI* **42**(2000) 861-883.
[7] P. Yuan, D. Gu, D. Dai, Particulate migration behavior and its mechanism during selective laser melting of TiC reinforced Al matrix nanocomposites, *MATER DESIGN* **82**(2015) 46-55.
[8] C. Panwisawas, C.L. Qiu, Y. Sovani, J.W. Brooks, M.M. Attallah, H.C. Basoalto, On the role of thermal fluid dynamics into the evolution of porosity during selective laser melting, *SCRIPTA MATER* **105**(2015) 14-17.
[9] D. Dai, D. Gu, Tailoring surface quality through mass and momentum transfer modeling using a volume of fluid method in selective laser melting of TiC/AlSi10Mg powder, *INT J. MACH TOOL MANU* **88**(2015) 95-107.
[10] S. Tammas-Williams, H. Zhao, F. Léonard, F. Derguti, I. Todd, P.B. Prangnell, XCT analysis of the influence of melt strategies on defect population in Ti–6Al–4V components manufactured by Selective Electron Beam Melting, *MATER CHARACT* **102**(2015) 47-61.

[11] S. Pang, W. Chen, J. Zhou, D. Liao, Self-consistent modeling of keyhole and weld pool dynamics in tandem dual beam laser welding of aluminum alloy, *J. MATER PROCESS TECH* **217**(2015) 131-143.
[12] B. Zhang, B. Li, Y. He, Growth kinetics of single inclusion in molten metal, *Journal of Iron and Steel Research* **17**(2005) 19-25.
[13] X. Zhou, D. Wang, X. Liu, D. Zhang, S. Qu, J. Ma, G. London, Z. Shen, W. Liu, 3D-imaging of selective laser melting defects in a Co–Cr–Mo alloy by synchrotron radiation micro-CT, *ACTA MATER* **98**(2015) 1-16.
[14] L.J. OBLONSKY, T.M. DEVINE, A SURFACE-ENHANCED RAMAN-SPECTROSCOPIC STUDY OF THE PASSIVE FILMS FORMED IN BORATE BUFFER ON IRON, NICKEL, CHROMIUM AND STAINLESS-STEEL, *CORROS SCI* **37**(1995) 17-41.
[15] L.F. Zhang, S. Taniguchi, K.K. Cai, Fluid flow and inclusion removal in continuous casting tundish, *METALL MATER TRANS B* **31**(2000) 253-266.
[16] X. Zhou, X. Liu, D. Zhang, Z. Shen, W. Liu, Balling Phenomena in Selective Laser Melted Tungsten, *J. MATER PROCESS TECH* **222**(2015) 33-42.